The Generalized Forward–Backward Method for Analyzing the Scattering from Targets on Ocean-Like Rough Surfaces

Marcos Rodríguez Pino, Luis Landesa, *Member, IEEE*, José Luis Rodríguez, Fernando Obelleiro, *Member, IEEE*, and Robert J. Burkholder, *Senior Member, IEEE*

***Abstract*— In a recent work, the iterative forward–backward (FB) method has been proposed to solve the magnetic field integral equation (MFIE) for smooth one-dimensional (1-D) rough surfaces. This method has proved to be very efficient, converging in a very small number of iterations. Nevertheless, this solution becomes unstable when some obstacle, like a ship or a large breaking wave, is included in the original problem. In this paper, we propose a new method: the generalized forward–backward (GFB) method to solve such kinds of complex problems. The approach is formulated for the electric field integral equation (EFIE), which is solved using a hybrid combination of the conventional FB method and the method of moments (MoM), the latter of which is only applied over a small region around the obstacle. The GFB method is shown to provide accurate results while maintaining the efficiency and fast convergence of the conventional FB method. Some numerical results demonstrate the efficiency and accuracy of the new method even for low-grazing angle scattering problems.**

***Index Terms*— Integral equations, iterative methods, remote sensing, rough-surface scattering, sea scattering.**

I. Introduction

THE electromagnetic (EM) scattering from rough surfaces such as ocean-like surfaces has been extensively treated in the literature. A recent review can be found in a special issue about this topic [1]. Most recent advances have been focused on the direct numerical simulation of the scattering problem. Numerical techniques based on integral equation formulations such as the well-known method of moments (MoM) [2] are apparently some of the few sufficiently accurate and robust methods for low-grazing-angle scattering problems and have played an increasingly important role.

Effects such as multiple scattering, shadowing, and diffraction, which are very difficult to model analytically, become more important as the incidence angle approaches the grazing limit. Furthermore, low-grazing angles require that a large region of the sea surface needs to be taken into account, which means that a large number of surface unknowns (N) must be considered and, therefore, more powerful numerical methods become necessary. Given that the usual approach to the random ocean surface problem is a Monte Carlo simulation in which the scattering statistics are generated over a large number of surface realizations, the computational cost becomes even more critical.

Different methods have been developed in recent years in order to reduce the number of computer operations required to analyze the rough-surface scattering problem via the method of moments. It is worth mentioning, among others, the banded matrix iterative approach/canonical grid (BMIA/CG method [3]–[9], based on splitting the field/surface current interaction into near-field and nonnear-field components; the solution is obtained by iteratively inverting the banded near-field interaction matrix, while correcting the solution with the far-field interaction. The nonnear-field interactions are expanded into a canonical grid, which is a horizontal surface in this case, so that the fast Fourier transform (FFT) can be applied. In a very recent work [10], the method has been also extended to treat scattering from one-dimensional (1-D) dielectric random rough surfaces at near-grazing angles.

A more general iterative solution based on a multigrid decomposition and the generalized conjugate residual (GCR) method, has been presented in [11]. This solution is not as efficient as BMIA/CG, but it is considerably faster than a direct solution and besides has the important benefit of a significant reduction in storage requirements.

Recently, a new and powerful iterative numerical technique called the forward–backward (FB) method has been proposed by Holliday *et al*. [12], [13] for solving the magnetic field integral equation (MFIE), which describes the current induced on a perfect electrically conducting (PEC) surface. A similar approach called the method of ordered multiple interactions (MOMI) has been simultaneously proposed by Kapp and Brown [14]. Both of them are based on splitting the current at each point into two components: the *forward* contribution due to the incident field and the radiation of the current elements located in front of the receiving element and the *backward* contribution due to the current elements located beyond the receiving element. The forward component is first found over the whole surface and then it is used to determine the backward contribution. This is repeated in an iterative process until a converged solution is reached. These methods have shown a very fast convergence, obtaining accurate results within very

Manuscript received September 16, 1998; revised March 16, 1999. This work was supported by the United States Office of Naval Research under Grant N00014-98-1-0243.

M. R. Pino, L. Landesa, J. L. Rodríguez, and F. Obelleiro are with the Dipartmento Tecnoloxías das Comunicacións, Universidade de Vigo, Campus Universitario s/n, Vigo, 36200 Spain.

R. J. Burkholder is with the ElectroScience Laboratory, The Ohio State University, Department of Electrical Engineering, Columbus, OH 43212 USA.

Publisher Item Identifier S 0018-926X(99)05802-0.

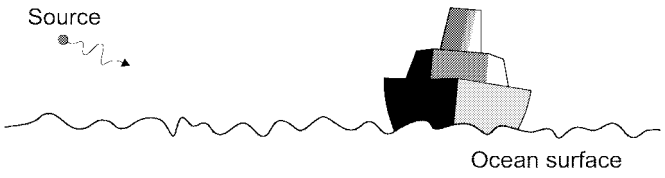

Fig. 1. A scattering obstacle on an ocean-like surface illuminated by a low-angle incident field.

few iterations, which makes them computationally effective. The operational count is $O(N^2)$ (*of order* N^2) and, thus, the simulation of quite large surfaces becomes possible, even for low-grazing angles of incidence.

In a recent paper [15], the MOMI method has been performed with the inclusion of a curvature term in the diagonal of the kernel matrix, in order to properly represent the propagator matrix. This helps to eliminate the undesired sampling sensitivity effect. In [16], the FB method is generalized to the scattering from imperfect conductors with dielectric constants near that of sea water at 1 GHz. Finally, in [17], a novel algorithm has been proposed which greatly accelerates the FB method based on the spectral representation of the Green's function. The computational cost and storage requirements are reduced to $O(N)$. It is noted that the acceleration technique may also be applied to the generalized method introduced in this paper, as discussed later.

A hybrid approach has been presented in [18] where the scattering from water waves of differing degrees of breaking is numerically examined by combining the MoM and the geometrical theory of diffraction (GTD). The technique is implemented using impedance-surface boundary conditions to handle scattering media of finite conductivity such as sea water.

In this paper, we present a generalization of the FB method which allows us to study the scattering from composite surfaces that can include one or more large arbitrarily shaped obstacles (like a ship or a large rogue breaking wave) on the ocean surface, as shown in Fig. 1. The conventional FB method is not expected to exhibit convergent behavior for such problems. The new approach, called the generalized forward–backward (GFB) method, is based on a combination of the conventional FB method with the MoM, where the MoM is only applied to the region close to the obstacle. The solution is found through an iterative procedure based on the same general concepts as the FB method, but with some significant differences. The computational cost of the GFB method is similar to the FB solution. It only includes an additional cost associated with the direct MoM solution of a small region containing the obstacle and nearby sea surface. The GFB method is very useful for predicting and studying the EM scattering from targets in the presence of a rough surface.

This paper is organized as follows. The conventional FB formulation for the solution of the electric field integral equation (EFIE) is presented in Section II. Section III develops the generalization of the previous method which leads to the new GFB iterative solution. Some numerical results are presented in Section IV and a summary and conclusions can be found in Section V. In the rest of the paper, the fields and the currents will be assumed to have a time-harmonic dependence of the form $e^{j\omega t}$, which will be suppressed from the field expressions. The radian frequency is ω, and μ and k are the permeability and wavenumber, respectively, of the medium above the rough surface (generally assumed to be free space).

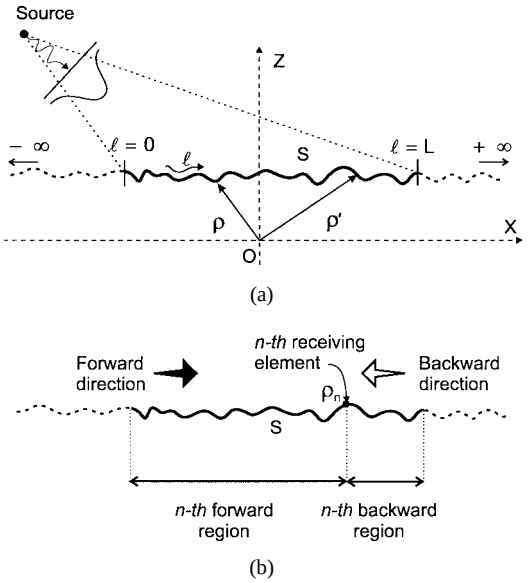

Fig. 2. (a) Ocean-like surface illuminated by a TM (E_y) polarized near-grazing incident field. (b) Forward and backward regions for the nth matching point.

II. The Conventional Forward–Backward Method for the Two-Dimensional EFIE Scattering Problem

The MFIE for a two-dimensional (2-D) scattering problem dealing with a 1-D rough surface and its solution by the FB method has been presented in [13]. Here we are concerned with the solution of the EFIE in a similar way. The application of the FB method combined with the EFIE has already been done in [17], where a new approach based on the spectral representation of the Green's function accelerates the computation of the forward and backward matrix–vector products. In this section, the formulation of the FB method is briefly reviewed, starting with the EFIE followed by a discretization process using the MoM to establish the corresponding matrix equations which will be solved in an iterative way.

Consider a 1-D ocean-like surface depicted in Fig. 2(a). The sea water is modeled here as a PEC material, so there is no penetration into the sea surface S. The permittivity and conductive lossiness of sea water at microwave frequencies are very high, so the PEC model is expected to be very accurate for radar scattering problems. This is especially true for low-grazing angles. The method may also be applied to impenetrable material surfaces without loss of generality.

The horizontal and vertical coordinates of the parametric surface of Fig. 2(a) are, respectively, $x(\ell)$ and $z(\ell)$, both functions of the path length ℓ on the surface. For such a surface, illuminated by a TM (E_y) polarized incident field, the EFIE can be obtained by imposing the tangential electric

field boundary condition on the PEC surface S

$$-\frac{\omega\mu}{4}\int_S J(\boldsymbol{\rho}')\,H_0^{(2)}(k|\boldsymbol{\rho}-\boldsymbol{\rho}'|)\,d\ell' = -E^i(\boldsymbol{\rho}) \tag{1}$$

where $E^i(\boldsymbol{\rho})$ is the incident field at a point $\boldsymbol{\rho} \in S$, $J(\boldsymbol{\rho}')$ is the induced current, and $H_0^{(2)}(k|\boldsymbol{\rho}-\boldsymbol{\rho}'|)$ is the second-kind Hankel function with order zero [2]. The current $J(\boldsymbol{\rho}')$ radiates in free-space and generates the scattered fields. This equation is to be solved through discretization by using the MoM. Although the surface S extends from minus infinity to infinity in x, the incident field is considered to be tapered so that the illuminated rough surface and, thus, the integration in (1) can be confined to a finite region of length L.

For our purposes, we will apply the most simple formulation of the MoM using a set of N pulse-basis functions and point-matching weighting at the center of each current element [2]. Typically, about ten pulse basis functions per wavelength are used. After the discretization process, (1) is transformed into a matrix equation

$$\bar{\bar{Z}}\cdot\bar{I} = \bar{V}. \tag{2}$$

The elements of the impedance matrix $\bar{\bar{Z}}$ are given by

$$Z_{mn} = \begin{cases} -\frac{\omega\mu}{4}\left[1 - j\frac{2}{\pi}\ln\left(\frac{\gamma k\Delta\ell}{4e}\right)\right]\Delta\ell & m = n \\ -\frac{\omega\mu}{4}\,H_0^{(2)}(k|\boldsymbol{\rho}_m-\boldsymbol{\rho}_n|)\Delta\ell & m \neq n \end{cases} \tag{3}$$

where γ is the Euler constant 0.577 216, $\Delta\ell$ is the width of the pulse basis and $\boldsymbol{\rho}_n$ is the position vector of the nth pulse-basis center. Matrix $\bar{I}$ is a column vector that contains the unknown coefficients $\bar{I} = \{I_n \mid n = 1,\ldots,N\}$ that are used to approximate the current

$$J(\boldsymbol{\rho}') \approx \sum_{n=1}^{N} I_n P_n(\boldsymbol{\rho}') \tag{4}$$

where $P_n(\boldsymbol{\rho}')$ denotes the unit pulse-basis function centered at $\boldsymbol{\rho}_n$. The column vector $\bar{V}$ elements are given by minus the incident field at the matching points

$$V_n = -E^i(\boldsymbol{\rho}_n). \tag{5}$$

For brevity, the expressions have been developed only for the TM (E_y) polarization. Similar equations can be easily derived for the TE polarization. Nevertheless, the FB method that will be described below is applicable to both polarizations.

The FB method will be formulated using the matrix notation of (2), instead of the integral equation (1). First, consider the following decomposition applied over the matrices involved in (2)

$$\bar{I} = \bar{I}^f + \bar{I}^b \tag{6}$$

$$\bar{\bar{Z}} = \bar{\bar{Z}}^f + \bar{\bar{Z}}^s + \bar{\bar{Z}}^b \tag{7}$$

where $\bar{I}^f$ is the forward component (i.e., the current contribution due to the waves propagating in the forward direction), $\bar{I}^b$ is the backward component (or current contribution due to the waves propagating in the backward direction), and $\bar{\bar{Z}}^f$, $\bar{\bar{Z}}^s$, and $\bar{\bar{Z}}^b$ are, respectively, the lower triangular part, the diagonal part (self impedance terms), and the upper triangular part of $\bar{\bar{Z}}$.

Using (6) and (7), (2) can now be split into forward-propagation and backward-propagation matrix equations, respectively, as follows:

$$\bar{\bar{Z}}^s\cdot\bar{I}^f = \bar{V} - \bar{\bar{Z}}^f\cdot(\bar{I}^f + \bar{I}^b) \tag{8}$$

$$\bar{\bar{Z}}^s\cdot\bar{I}^b = -\bar{\bar{Z}}^b\cdot(\bar{I}^f + \bar{I}^b). \tag{9}$$

Here, (8) has been assumed by definition to describe the forward-propagation, so (9) then follows from (2), (6), and (7) and describes the backward propagation. It can be seen that for a given nth matching point located at $\boldsymbol{\rho}_n$, the right-hand side (RHS) of (8) contains the incident field and the contribution of the current elements located in the front of this receiving element, which corresponds to the nth forward region in Fig. 2(b). Likewise, the RHS of (9) contains the influence of the current elements in the rear of the receiving element, so it represents the nth backward region contribution as in Fig. 2(b). From this it is clear that *the MoM current elements must be numbered sequentially as a function of increasing x in the FB method*, i.e.,

$$x(\boldsymbol{\rho}_{n-1}) < x(\boldsymbol{\rho}_n) < x(\boldsymbol{\rho}_{n+1}). \tag{10}$$

Equations (8) and (9) can be solved iteratively, where the currents in the ith stage of the algorithm $(\bar{I}^{f,(i)}, \bar{I}^{b,(i)})$ are obtained as

$$(\bar{\bar{Z}}^s + \bar{\bar{Z}}^f)\cdot\bar{I}^{f,(i)} = \bar{V} - \bar{\bar{Z}}^f\cdot\bar{I}^{b,(i-1)} \tag{11}$$

$$(\bar{\bar{Z}}^s + \bar{\bar{Z}}^b)\cdot\bar{I}^{b,(i)} = -\bar{\bar{Z}}^b\cdot\bar{I}^{f,(i)}. \tag{12}$$

The algorithm starts with $\bar{I}^{b,(0)} = 0$. It must be noticed that the matrices involved in this iterative process do not need to be factorized or inverted because $\bar{\bar{Z}}^s + \bar{\bar{Z}}^f$ is a lower triangular matrix and $\bar{\bar{Z}}^s + \bar{\bar{Z}}^b$ is an upper triangular matrix; so, (11) and (12) can be solved for $\bar{I}^{f,(i)}$ and $\bar{I}^{b,(i)}$ by forward and backward substitution, respectively. The convergence has been shown to be extremely rapid for moderately rough surfaces, generally requiring fewer than ten iterations. However, it should be noted that the algorithm may become unstable for re-entrant surfaces, i.e., for surfaces where $x(\boldsymbol{\rho}_{n+1}) \leq x(\boldsymbol{\rho}_n)$ for one or more points $\boldsymbol{\rho}_n$. This violates the sequential number requirement of (10). The GFB method developed next overcomes this limitation for the case of one or more arbitrarily shaped scattering obstacles on the surface.

III. The Generalized Forward–Backward Method

Consider now the composite problem depicted in the Fig. 3, where one or more PEC obstacles (like a ship or large rogue breaking wave) are included in the surface contour S. For this kind of problem the conventional FB method does not exhibit convergent behavior, because the presence of the obstacle highly disturbs the propagation process assumed by the conventional FB method. There are strong interactions between the obstacle and the nearby ocean-like surface, and within the obstacle itself, all of which may not be taken into account with the conventional formulation involved in the standard FB method.

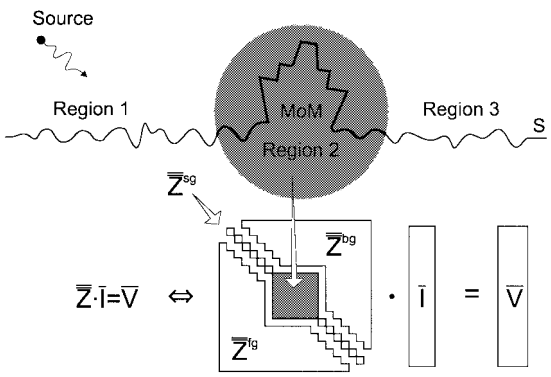

Fig. 3. Composite problem and matrix decomposition in the GFB method.

In order to overcome this drawback, the GFB method is presented in this paper. The GFB method consists of a generalization of the conventional FB approach which enhances the scope of application of the previous method to composite scattering problems as the one depicted in Fig. 3. This method is based on the same general concepts previously stated for the FB method, but includes some significant differences mainly in the decomposition of the matrix $\bar{\bar{Z}}$ that will be detailed next. For the sake of simplicity, the GFB formulation will be presented for a simple problem consisting of a sea surface containing only one obstacle (see Fig. 3); the extension of the formulation to several obstacles is obvious as will be seen later.

Again starting with (2), which has been obtained from (1) after the MoM discretization process. In the same way as done in the FB method, the current is expressed as the sum of two contributions (*forward* and *backward*)

$$\bar{I} = \bar{I}^f + \bar{I}^b \tag{13}$$

but now the impedance matrix is split in a different way

$$\bar{\bar{Z}} = \bar{\bar{Z}}^{fg} + \bar{\bar{Z}}^{sg} + \bar{\bar{Z}}^{bg} \tag{14}$$

where the $\bar{\bar{Z}}^{sg}$ matrix is the diagonal part of $\bar{\bar{Z}}$ with an additional block including the impedance submatrix corresponding to the ship and nearby sea region (Region 2 in Fig. 3); while $\bar{\bar{Z}}^{fg}$ and $\bar{\bar{Z}}^{bg}$ are, respectively, the lower triangular part and the upper triangular part of $\bar{\bar{Z}}$ but excluding the matrix $\bar{\bar{Z}}^{sg}$, as illustrated in Fig. 3. With this decomposition, matrix $\bar{\bar{Z}}^{sg}$ contains both the self (diagonal) terms and the interaction of the whole obstacle and nearby sea region together.

Then, the original system is transformed in a similar way as in the conventional FB method, yielding the following matrix equations:

$$\bar{\bar{Z}}^{sg}\cdot\bar{I}^f = \bar{V} - \bar{\bar{Z}}^{fg}\cdot(\bar{I}^f + \bar{I}^b) \tag{15}$$

$$\bar{\bar{Z}}^{sg}\cdot\bar{I}^b = -\bar{\bar{Z}}^{bg}\cdot(\bar{I}^f + \bar{I}^b) \tag{16}$$

which can be iteratively solved for $\bar{I}^{f,(i)}$ and $\bar{I}^{b,(i)}$ as

$$(\bar{\bar{Z}}^{sg} + \bar{\bar{Z}}^{fg})\cdot\bar{I}^{f,(i)} = \bar{V} - \bar{\bar{Z}}^{fg}\cdot\bar{I}^{b,(i-1)} \tag{17}$$

$$(\bar{\bar{Z}}^{sg} + \bar{\bar{Z}}^{bg})\cdot\bar{I}^{b,(i)} = -\bar{\bar{Z}}^{bg}\cdot\bar{I}^{f,(i)} \tag{18}$$

starting with $\bar{I}^{b,(0)} = 0$ in (17).

The solution of (17) and (18) differs from (11) and (12) because neither $\bar{\bar{Z}}^{sg} + \bar{\bar{Z}}^{fg}$ nor $\bar{\bar{Z}}^{sg} + \bar{\bar{Z}}^{bg}$ are triangular matrices. Nevertheless, the equations can also be easily solved by combining forward or backward substitution together with the direct factorization of the square block of $\bar{\bar{Z}}^{sg}$ whose dimension depends only on the number of current elements in Region 2, namely the ship and nearby sea (see Fig. 3). A description of the solution procedure can be found in the Appendix. Qualitatively, the solution proceeds as follows. For each iteration i:

1) find $\bar{I}^{f,(i)}$ over Region 1 using the forward propagation principle;
2) direct solve for $\bar{I}^{f,(i)}$ over Region 2 using the fields radiated by the Region 1 currents plus the incident field as excitation;
3) find $\bar{I}^{f,(i)}$ over Region 3 by the forward propagation principle;
4) find $\bar{I}^{b,(i)}$ over Region 3 by the backward propagation principle;
5) direct solve for $\bar{I}^{b,(i)}$ over Region 2 using the fields radiated by the Region 3 currents;
6) find $\bar{I}^{b,(i)}$ over Region 1 using the backward propagation principle.

The computational cost of the GFB method is practically the same as the conventional FB method. It only has the additional computational cost of factorizing the square block of $\bar{\bar{Z}}^{sg}$, which corresponds to the MoM matrix of Region 2. Nevertheless, due to the limited size of this block matrix, its factorization can be performed once and stored, thus reducing the computational work in subsequent iterations and for other excitations. So, it can be concluded that the GFB method has a computational cost of $O(N^2)$ per iteration as in the FB method [17]. The storage requirement is $O(N)$ to store the iterated currents as in the FB method with the additional storage of a square matrix of size $M \times M$, where M is the number of current elements included in the MoM region (Region 2 in Fig. 3). Generally, $M \ll N$ but the $O(M^2)$ matrix storage requirement may be comparable to the $O(N)$ storage of the currents. It is noted that the $O(N)$ storage requirement assumes that the full $\bar{\bar{Z}}$ matrix is not stored, so it is necessary to recompute the matrix elements at each iteration (except for the inner MoM matrix associated with Region 2). However, the simple closed form of the matrix elements allows them to be computed very quickly, and the number of iterations is usually very small (typically less than ten). Finally, it is noted that the new spectral technique introduced in [17] for accelerating the FB method may likewise be used to accelerate the GFB method with some minor modifications.

IV. Numerical Results

In this section, results are presented to validate the convergence and accuracy of the new GFB method and to investigate some of the effects of a random rough surface on the backscatter pattern of a target on the surface. In the following, the sea surfaces are randomly generated using a Pierson–Moskowitz wave model for a given wind speed [19]. The excitation antenna is a linear array of 15 equally spaced

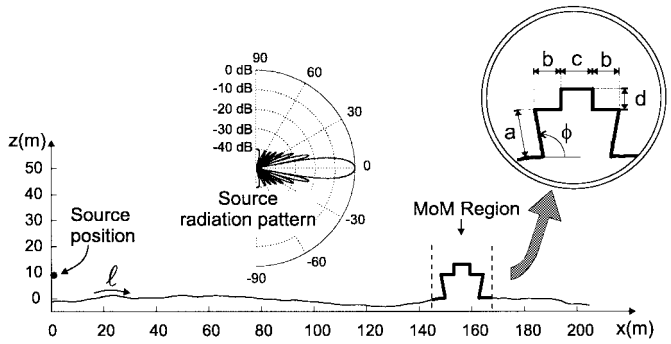

Fig. 4. Source and target geometry on a sea surface with wind speed 15 m/s. Target dimensions: $a = 9.14$, $b = 5$, $c = 4$, $d = 6$, $\phi = 100^{\circ}$. Units are in meters.

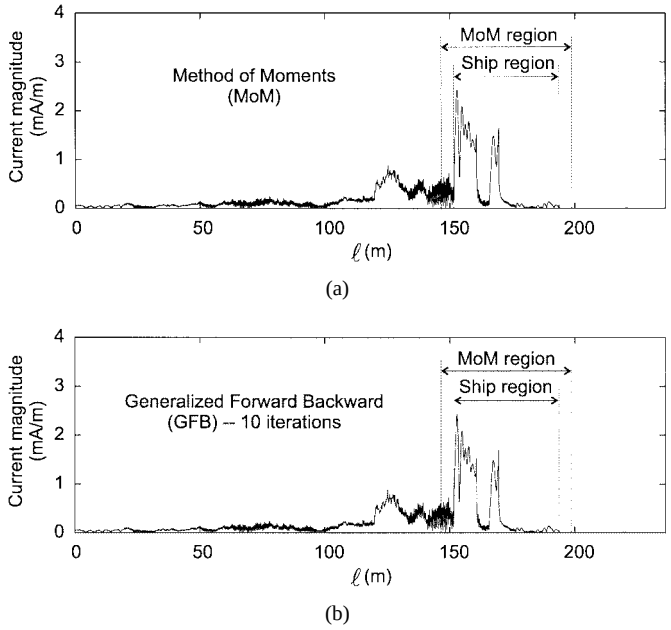

Fig. 5. Magnitude of the currents as a function of ℓ. (a) The moment method. (b) The GFB method (tenth iteration).

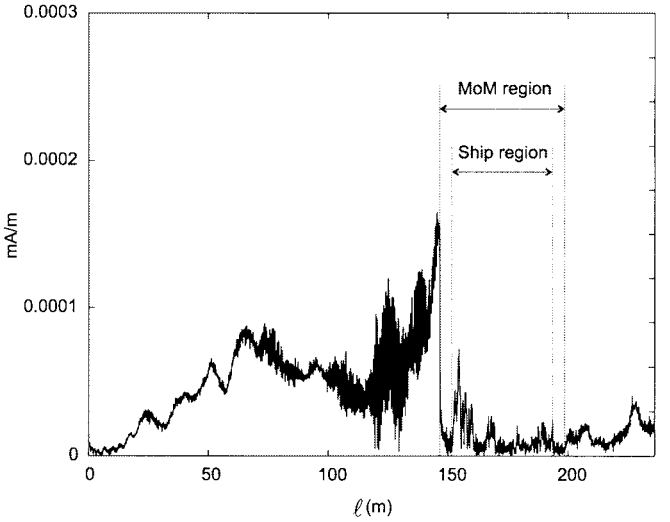

Fig. 6. Magnitude of the difference between GFB and MoM currents as a function of ℓ.

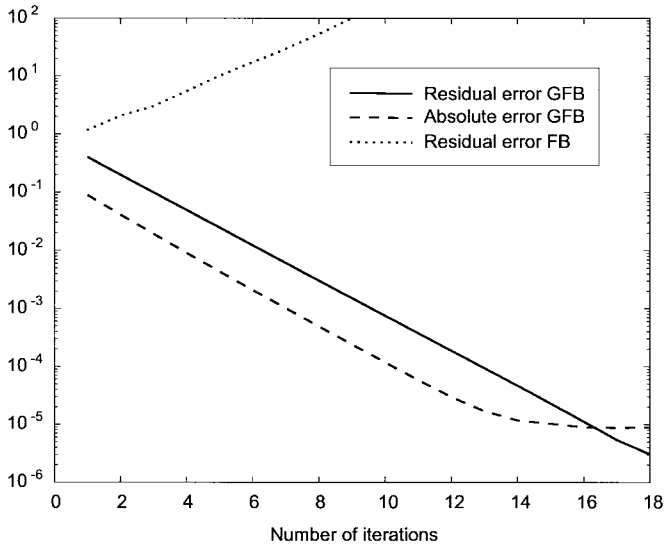

Fig. 7. Residual and absolute errors versus the number of iterations.

electric line sources with a cosine aperture weighting function. This source array produces a 9° main beam with low sidelobes. (Low sidelobes are important so that the sea surface near the source is not strongly illuminated). The polarization is horizontal, as in the derivation for the TM EFIE earlier.

Fig. 4 shows the source location and pattern function relative to a PEC ship-like target on a PEC rough sea surface. For this example, the sea surface is 204.8 m in length, the wind speed is 15 m/s, and the wavelength is 1 m. The wave height for a wind speed of 15 m/s is about 3 m, which corresponds to Sea State 5 of the World Meteorological Organization (WMO). The source is 10 m high on the extreme left and points horizontally. The MoM region shown within the dashed vertical lines contains the ship and 5 m of sea surface on either side. For validating the new method with this example, the current obtained with GFB is compared with the solution given by MoM applied to the whole surface in Fig. 5, as a function of ℓ. For the GFB results, the MoM region is within the outer dashed vertical lines, and the ship is within the inner dashed lines. Ten iterations are used. The difference between the two currents is shown in the Fig. 6. After only ten iterations, the maximum difference in the currents is on the order of 10^{-4} mA/m.

The residual error is used for monitoring the convergence of the GFB in terms of the number of iterations. The residual error vector after the ith iteration is defined as

$$\bar{r}^{(i)} = \bar{V} - \bar{\bar{Z}} \cdot \bar{I}^{(i)}. \tag{19}$$

By substituting (17) and (18) in (19), the residual error vector can be evaluated in a more efficient way as

$$\bar{r}^{(i)} = \bar{\bar{Z}}^{fg} \cdot \left[\bar{I}^{b(i-1)} - \bar{I}^{b(i)}\right]. \tag{20}$$

The residual error is defined as

$$\textit{residual error} = \frac{\left|\left|\bar{r}^{(i)}\right|\right|}{\left|\left|\bar{V}\right|\right|} \tag{21}$$

where $||\bar{r}^{(i)}||$ denotes the vector norm. The residual error of the GFB for this example is shown in Fig. 7; it decreases

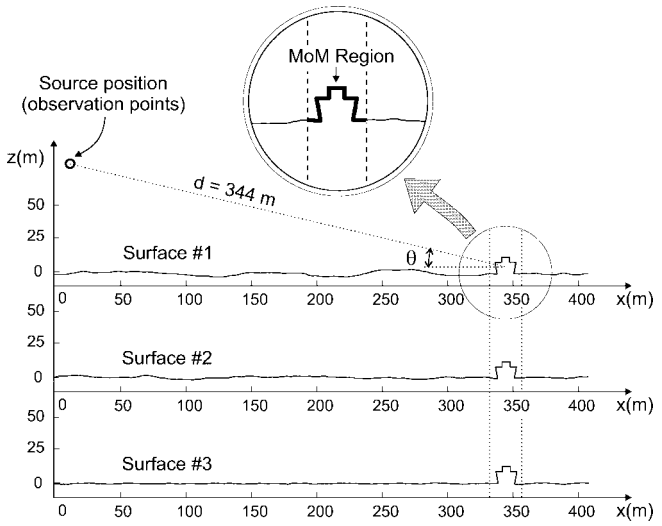

Fig. 8. Geometry for backscatter patterns. Wind speed is 15 m/s for Surfaces #1 and #2, and 7 m/s for Surface #3. The ship is the same in all three cases.

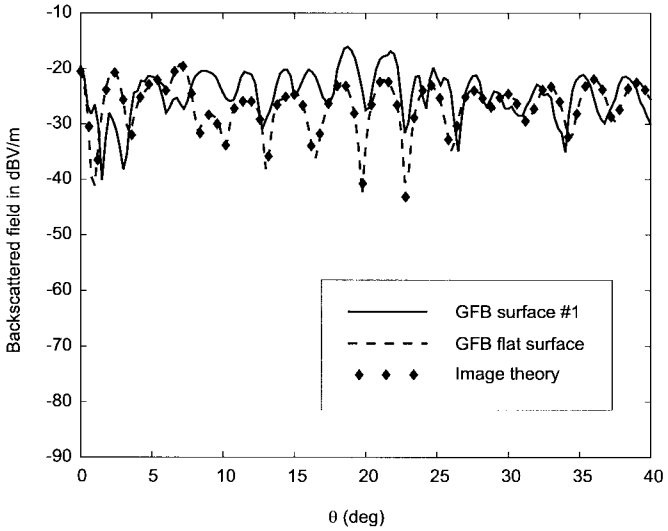

Fig. 9. Comparison between the backscattered field of a ship on a rough surface (Surface #1) and on a flat surface. A reference solution for an infinite flat surface found using MoM and image theory is also included.

exponentially with the number of iterations. The residual error of the FB method has also been plotted and as for reasons explained in Section III, the FB method generally cannot achieve a convergent solution when an obstacle is present in the sea surface. Fig. 7 also plots the absolute error of the GFB method, defined by

$$\textit{absolute error} = \frac{\left\|\bar{I}^{(i)} - \bar{I}_{\mathrm{MoM}}\right\|}{\left\|\bar{I}_{\mathrm{MoM}}\right\|} \tag{22}$$

where $\bar{I}_{\mathrm{MoM}}$ is the MoM reference solution for the currents. It is seen that the absolute error also falls exponentially, but after about 14 iterations it levels out. This is often a characteristic of iterative methods in general and is caused by the finite numerical precision of the computer. To judge convergence of the solution, the residual error is a very good indicator and is easy to compute at each iteration using (20) and (21). Halting the algorithm when the residual error reaches about 10^{-2} or 10^{-3} yields very accurate scattering results. For this example, 6–10 iterations is found to be quite sufficient.

To investigate the scattering behavior of a ship on a rough surface, the geometry of Fig. 8 is considered. The ship and the source are the same as in Fig. 4, but the length of the sea surface is 409.6 m and the source antenna moves in elevation at a constant distance from the ship to generate a backscatter pattern (i.e., the pattern of the scattered field at the source position as a function of elevation angle). The antenna beam points directly at the ship and the source starts at a height of 10 m above the surface. The wavelength is again 1 m. Three different randomly generated sea surfaces are shown in the figure. Surfaces #1 and #2 are at a wind speed of 15 m/s and Surface #3 is at 7 m/s. The wave height is 1.4 m for wind speed 7 m/s, which corresponds to Sea State 4 of the WMO. It is noted that the ship remains upright and does not roll with the waves in the results that follow.

Fig. 9 shows the backscatter patterns for the ship on Surface #1 and for the ship on a finite flat surface of the same length for comparison. Also shown is a reference MoM solution for the ship on an infinite flat surface found using image theory.

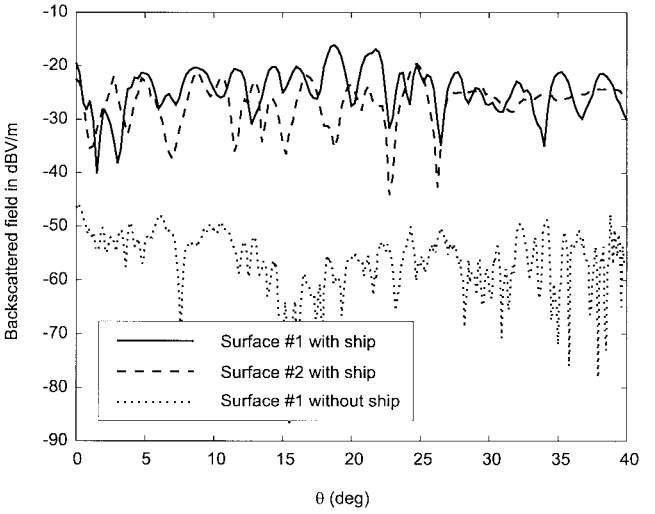

Fig. 10. Comparison between the backscattered field for Surfaces #1 and #2 with the ship. The backscattering from surface #1 without the ship is also plotted.

The very close agreement between the image theory result and the GFB result for the finite flat surface show that end-point effects are negligible, and further validates the GFB method for scattering problems. The figure also shows that the rough surface greatly affects the backscatter pattern compared with a flat surface.

Fig. 10 shows the backscatter patterns for the ship on the two rough surfaces depicted in Fig. 8. It is seen that the patterns are significantly different for these two surfaces that have the same roughness scale, although it could be argued that the patterns are at about the same average level. The backscatter due to Surface #1 without the ship is also plotted to show the level of the background clutter for this wind speed. The clutter level computed here is quite low, but it should be mentioned that this ocean model does not include the effects of breaking waves that generally dominate the backscatter return

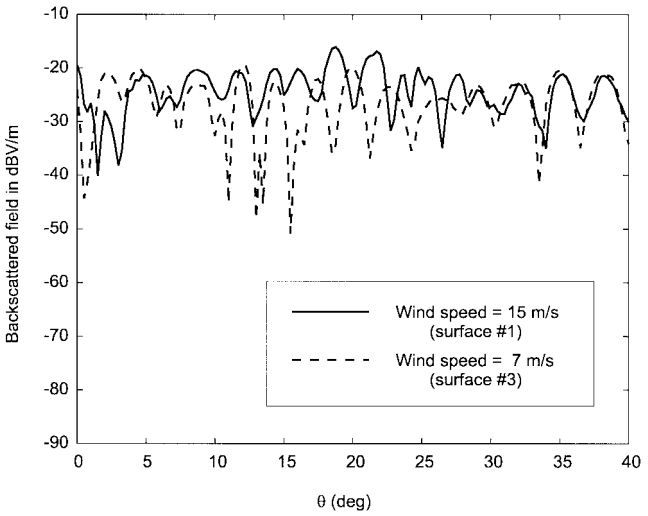

Fig. 11. Comparison between the backscattered field for a ship on Surface #1 and on a randomly generated surface with wind speed = 7 m/s.

from the ocean in the absence of a ship. In fact, the clutter level is due almost entirely to direct reflection of the downward pointing low-sidelobe beams. However, as noted earlier, the GFB method could be used to analyze an isolated breaking wave in the presence of an otherwise smoothly varying ocean surface simply by replacing the ship geometry with that of the wave.

Fig. 11 shows the backscatter patterns for the ship on Surface #1 and on a randomly generated surface with wind speed 7 m/s. Again, the patterns are significantly different although they are at about the same average level. Furthermore, the 7 m/s result does not appear any closer to the flat surface result of Fig. 9 than the 15 m/s result, even though the roughness scale is smaller. Any further conclusions about these results requires a more thorough statistical study, which is beyond the goals of this paper.

V. Discussion and Conclusions

In this paper, we have presented a new computational algorithm, the GFB method, which enhances the scope of application of the conventional FB method to composite 2-D scattering problems consisting of a randomly varying smooth ocean-like surface with abrupt target obstacles present like ships, rogue waves, etc. The new approach has been shown to provide very accurate results and maintains the same fast convergence (usually in less than ten iterations) and $O(N^2)$ computational cost associated with the conventional FB solution. The storage requirement is $O(N+M^2)$, where M is the number of basis functions used in the small MoM region around the target. Nevertheless, the $O(N^2)$ computational cost makes the method inefficient for very large surfaces. In order to overcome this limitation, the GFB could be combined with modern integral equation acceleration algorithms such as the asymptotic fast multipole method [20] or the novel spectral acceleration method [17], which could reduce the computational cost to $O(N)$. The improvement of the GFB method, combining it with novel acceleration algorithms, will be addressed in a future submission.

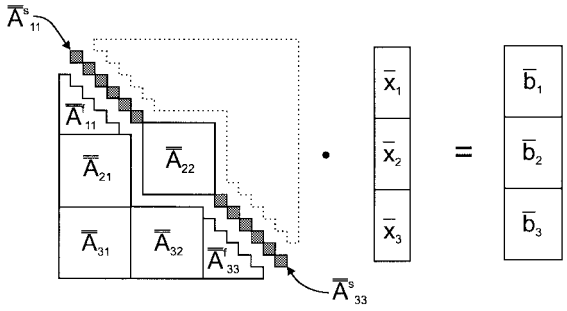

Fig. 12. Block decomposition of a "quasi" lower triangular matrix.

The numerical results show that different random ocean surfaces greatly affect the backscatter patterns of a ship-like target, although the patterns tend to have about the same average level. It is difficult to make any further conclusions at this point about how the wind speed affects the backscatter patterns. One would expect, for example, that higher wind speeds (and, therefore, larger roughness scales) would cause a larger variance in the backscatter. A more thorough statistical investigation is necessary, which is beyond the scope of this paper. The purpose of the GFB method introduced here is to provide a numerical tool for studying this class of scattering problems; the Monte Carlo simulations will be considered in a future submission.

Appendix

In this Appendix, a description of the procedure used to solve (17) and (18) is presented. It must be pointed out that neither $\bar{\bar{Z}}^{sg}+\bar{\bar{Z}}^{fg}$ nor $\bar{\bar{Z}}^{sg}+\bar{\bar{Z}}^{bg}$ are triangular matrices; nevertheless, these equations can be easily solved by combining forward or backward substitution together with the direct factorization of a square-block submatrix whose dimension is just the extent of the MoM region. For brevity, we will explain only the resolution of (17) which concerns the matrix $\bar{\bar{Z}}^{sg}+\bar{\bar{Z}}^{fg}$. Equation (18) can be solved in a similar way.

Equation (17) has the general form

$$\bar{\bar{A}}\cdot\bar{x}=\bar{b} \tag{23}$$

where $\bar{\bar{A}}=\bar{\bar{Z}}^{sg}+\bar{\bar{Z}}^{fg}$, $\bar{x}=\bar{I}^{f,(i)}$, and $\bar{b}=\bar{V}-\bar{\bar{Z}}^{fg}\cdot\bar{I}^{b,(i-1)}$. $\bar{\bar{A}}$ is a "quasi" lower triangular matrix as depicted in Fig. 12. In order to solve these equations in an efficient way, the matrices $\bar{\bar{A}}$, $\bar{x}$, and $\bar{b}$ of (23) are subdivided into blocks as shown in Fig. 12. Thus (23) can be expressed in terms of the blocks as follows:

$$\left(\bar{\bar{A}}^{s}_{11}+\bar{\bar{A}}^{f}_{11}\right)\cdot\bar{x}_1=\bar{b}_1 \tag{24}$$

$$\bar{\bar{A}}_{21}\cdot\bar{x}_1+\bar{\bar{A}}_{22}\cdot\bar{x}_2=\bar{b}_2 \tag{25}$$

$$\bar{\bar{A}}_{31}\cdot\bar{x}_1+\bar{\bar{A}}_{32}\cdot\bar{x}_2+\left(\bar{\bar{A}}^{s}_{33}+\bar{\bar{A}}^{f}_{33}\right)\cdot\bar{x}_3=\bar{b}_3 \tag{26}$$

The solution is then obtained as follows.

1) Equation (24) is a lower triangular matrix, so $\bar{x}_1$ can be easily obtained by forward substitution.

2) Once $\bar{x}_1$ is has been calculated, $\bar{x}_2$ can be obtained from (25) by the direct solution of

$$\bar{\bar{A}}_{22} \cdot \bar{x}_2 = (\bar{b}_2 - \bar{\bar{A}}_{21} \cdot \bar{x}_1). \tag{27}$$

LU decomposition may be used so that $\bar{\bar{A}}_{22}$ needs to be factorized only once for a given Region 2 geometry. The factorized matrix may then be saved for subsequent iterations and for other excitations.

3) Finally, once $\bar{x}_1$ and $\bar{x}_2$ have been calculated, $\bar{x}_3$ can be obtained from (26) again by forward substitution from

$$\left(\bar{\bar{A}}^s_{33} + \bar{\bar{A}}^f_{33}\right) \cdot \bar{x}_3 = \bar{b}_3 - \bar{\bar{A}}_{31} \cdot \bar{x}_1 - \bar{\bar{A}}_{32} \cdot \bar{x}_2 \tag{28}$$

because $\bar{\bar{A}}^s_{33} + \bar{\bar{A}}^f_{33}$ is a lower triangular matrix.

A similar procedure is applied for the solution of (18). The only difference is that in this case we will define upper triangular component matrices that can be solved by back substitution.

REFERENCES

[1] E. G. S. Brown, "Special issue on low-grazing-angle backscattering from rough surfaces," *IEEE Antennas Propagat*, vol. 46, pp. 2028–2031, Jan. 1998.

[2] R. F. Harrington, *Field Computation by Moment Method*. New York: IEEE Press, 1993.

[3] L. Tsang, C. H. Chang, and H. Sangani, "A banded matrix iterative approach to Monte Carlo simulations of scattering of waves by large-scale random rough surface problems: TM case," *Electron. Lett.*, vol. 29, pp. 166–167, Jan. 1993.

[4] L. Tsang, C. H. Chang, H. Sangani, A. Ishimaru, and P. Phu, "A banded matrix iterative approach to Monte Carlo simulations of large-scale random rough surface scattering: TE case," *J. Electromagn. Waves Applicat.*, vol. 7, no. 9, pp. 1185–1200, 1993.

[5] L. Li, C. H. Chang, and L. Tsang, "Numerical simulation of conical diffraction of tapered electromagnetic waves from random rough surfaces and applications to passive remote sensing," *Radio Sci.*, vol. 29, pp. 587–598, May/June 1994.

[6] L. Tsang, C. H. Chang, K. Pak, and H. Sangani, "Monte Carlo simulations of large-scale problems of random rough surface scattering and applications to grazing incidence with the BMIA/canonical grid method," *IEEE Trans. Antennas Propagat.*, vol. 43, pp. 851–859, Aug. 1995.

[7] K. Pak, L. Tsang, and J. T. Johnson, "Numerical simulations and backscattering enhancement of electromagnetic waves from two-dimensional electric random surface with the sparse-matrix canonical grid method," *J. Opt. Soc. Amer.*, vol. 14, pp. 1515–1529, 1995.

[8] J. T. Johnson, L. Tsang, R. T. Shin, K. Pak, C. H. Chang, A. Ishimaru, and Y. Kuga, "Backscattering enhancement of electromagnetic waves from two-dimensional perfectly conducting random rough surfaces: A comparison of Monte Carlo simulations with experimental data," *IEEE Trans. Antennas Propagat.*, vol. 44, pp. 748–756, May 1996.

[9] J. T. Johnson, "A numerical study of low-grazing angle backscattering from ocean-like impedance surfaces with the Canonical Grid method," *IEEE Trans. Antennas Propagat.*, vol. 46, pp. 114–120, Jan. 1998.

[10] C. H. Chan, L. Tsang, and Q. Li, "Monte Carlo simulations of large-scale one dimensional random rough-surface scattering at near-grazing incidence: Penetrable case," *IEEE Trans. Antennas Propagat.*, vol. 46, pp. 142–149, Jan. 1998.

[11] D. J. Donohue, H.-C. Ku, and D. R. Thompson, "Application of iterative Moment-Method solutions to ocean surfaces radar scattering," *IEEE Trans. Antennas Propagat.*, vol. 46, pp. 121–132, Jan. 1998.

[12] D. Holliday, L. L. DeRaad, and G. J. St-Cyr, "Volterra approximation for low grazing angle shadowing ocean-like surfaces," *IEEE Trans. Antennas Propagat.*, vol. 43, pp. 1199–1206, Nov. 1995.

[13] ——, "Forward–backward: A new method for computing low-grazing angle scattering," *IEEE Trans. Antennas Propagat.*, vol. 44, pp. 722–729, May 1996.

[14] D. A. Kapp and G. S. Brown, "A new numerical method for rough surface scattering calculations," *IEEE Trans. Antennas Propagat.*, vol. 44, pp. 711–721, May 1996.

[15] J. V. Toporkov, R. T. Mar.and, and G. S. Brown, "On the discretization of the integral equation describing scattering by rough conducting surfaces," *IEEE Trans. Antennas Propagat.*, vol. 46, pp. 150–161, Jan. 1998.

[16] D. Holliday, L. L. DeRaad, and G. J. St-Cyr, "Forward–backward method for scattering from imperfect conductors," *IEEE Trans. Antennas Propagat.*, vol. 46, pp. 101–107, Jan. 1998.

[17] H.-T. Chou and J. T. Johnson, "A novel acceleration algorithm for the computation of scattering from rough surfaces with the forward-backward method," *Radio Sci.*, to be published.

[18] J. C. West, J. M. Sturm, and S.-J. Ja, "Low-Grazing scattering from breaking water waves using an impedance boundary MM/GTD approach," *IEEE Trans. Antennas Propagat.*, vol. 46, pp. 93–100, Jan. 1998.

[19] W. J. Pierson and L. Moskowitz, "A proposed spectral form for fully developed wind seas based on the similarity theory of S. A. Kitaigorodskii," *J. Geophys. Res.*, vol. 69, pp. 5181–5190, 1964.

[20] R. J. Burkholder and D.-H. Kwon, "High-frequency asymptotic acceleration of the fast multipole method," *Radio Sci.*, vol. 51, pp. 1199–1206, Oct. 1996.

Marcos Rodríguez Pino was born in Vigo, Spain, in November 1972. He received the M.Sc. degree in telecommunication engineering from the University of Vigo, Spain, in 1997. He is currently working toward the Ph.D. degree at the same university.

In 1998, he worked as Visiting Scholar at the ElectroScience Laboratory, The Ohio State University, Columbus. His current research interests are applied mathematics and numerical techniques for computational electromagnetics.

Luis Landesa (M'98) was born in Vigo, Spain, in November 1971. He received the M.Sc. and the Ph.D. degrees in electrical engineering from the University of Vigo, Spain, in 1995 and 1998, respectively.

He is currently Assistant Researcher with the Departament of Tecnoloxías das Comunicacións at the University of Vigo, where he teaches practical courses in antennas. His current research interests are applied mathematics, computational electromagnetics, array antenna synthesis, inverse problems, and bio-electromagnetics.

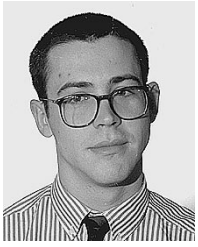

José Luis Rodríguez was born in Monforte de Lemos, Spain, in June 1967. He received the M.S. and Ph.D. degrees in telecommunication engineering from the University of Vigo, Spain, in 1992 and 1997, respectively.

He is currently enrolled in the University of Vigo, where he teaches courses about radar and remote sensing. During 1993 he was a Visiting Researcher at the ElectroScience Laboratory, The Ohio State University, Columbus. His areas of interest include computational electromagnetics, numerical analysis, and radar cross-section measurements.

Fernando Obelleiro (M'95) was born in Forcarei, Galiza, Spain, in April 1968. He received the M.Sc. and Ph.D. degrees in telecommunication engineering from the University of Vigo, Spain, in 1991 and 1994, respectively.

He is currently an Assistant Professor with the Department of Tecnoloxías das Comunicacións at the University of Vigo, where he teaches courses in electromagnetics fields and radar. During 1993 he was a Visiting Researcher at the ElectroScience Laboratory, The Ohio State University, Columbus. His current research interests are radar technology, radiation hazards, applied mathematics, and numerical techniques for computational electromagnetics.

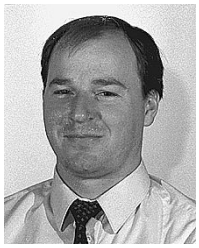

Robert J. Burkholder (S'85–M'89–SM'97) received the B.S., M.S., and Ph.D. degrees in electrical engineering from The Ohio State University, Columbus, in 1984, 1985, and 1989, respectively.

From 1989 to the present, he has been with The Ohio State University ElectroScience Laboratory, Department of Electrical Engineering, where he currently holds the titles of Research Scientist and Adjunct Associate Professor. His research specialties are high-frequency asymptotic techniques and their hybrid combination with numerical techniques for solving large-scale electromagnetic radiation and scattering problems. He has contributed extensively to the electromagnetic analysis of large cavities such as jet inlets/exhausts and is currently working on the more general problem of electromagnetic radiation, propagation, and scattering in realistically complex environments.

Dr. Burkholder is a member of URSI Commission B and a member of the Applied Computational Electromagnetics Society (ACES).